Efficiency/Predictability of 4D Trajectories at Tactical Level

Deliverable 4.2

TBO-Met

Grant:	**699294**
Call:	**H2020-SESAR-2015-1**
Topic:	**Sesar-04-2015 - Environment and Meteorology in ATM**
Consortium coordinator:	**Universidad de Sevilla**
Edition date:	**31 August 2017**
Edition:	**00.01.00**

Founding Members

EUROPEAN UNION EUROCONTROL

SESAR JOINT UNDERTAKING

Authoring & Approval

Authors of the document

Name/Beneficiary	Position/Title	Date
Daniel Sacher / MetSol	Task Leader	18/08/2017
Manuel Soler / UC3M	WP leader	30/08/2017
Juan Simarro / AEMET	AEMET Contribution Leader	30/08/2017

Reviewers internal to the project

Name/Beneficiary	Position/Title	Date
Thomas Hauf / MetSol	Scientific Advisor	28/08/2017
Jürgen Lang / MetSol	MetSol Leader	28/08/2017
Damian Rivas / USE	USE Contribution Leader	28/08/2017
Carl-Herbert Rokitansky / PLUS	PLUS Contribution Leader	28/08/2017

Approved for submission to the SJU By — Representatives of beneficiaries involved in the project

Name/Beneficiary	Position/Title	Date
Daniel Sacher / MetSol	Task Leader	31/08/2017
Manuel Soler / UC3M	WP leader	31/08/2017
Juan Simarro / AEMET	AEMET Contribution Leader	31/08/2017
Damian Rivas / USE	Project Coordinator	31/08/2017

Rejected By - Representatives of beneficiaries involved in the project

Name/Beneficiary	Position/Title	Date

Document History

Edition	Date	Status	Author	Justification
00.00.01	15/05/2017	Initial Draft	Daniel Sacher	New Document
00.00.04	18/08/2017	Reviewed Draft	Daniel Sacher	Updated Document
00.00.05	28/08/2017	Reviewed Draft	Manuel Soler	Updated Document
00.01.00	31/08/2017	First Issue	Manuel Soler	Updated Document

TBO-Met

METEOROLOGICAL UNCERTAINTY MANAGEMENT FOR TRAJECTORY BASED OPERATIONS

This Deliverable (D4.2) is part of a project that has received funding from the SESAR Joint Undertaking under grant agreement No 699294 under European Union's Horizon 2020 research and innovation programme.

Abstract

A major challenge for Trajectory-Based Operations is the existence of significant uncertainties in the models and systems required for trajectory prediction. In particular, weather uncertainty has been acknowledged as one of the most (if not the most) relevant ones. In this deliverable we present results on robust trajectory planning at the tactical level (short-term planning and execution). Uncertainty associated to the evolution of thunderstorms is assumed to be the unique source of uncertainty. State-of-the-art short-term forecasts (also referred to as nowcasts) are used as input data for the uncertain evolution of thunderstorms. The main goal is to re-plan trajectories that are efficient, yet safe in avoiding the storms considering that its evolution is uncertain. Robust trajectories (computed at the pre-tactical phase) are used as reference trajectories. Should these trajectories overfly a volume of airspace with storm activity, a trajectory is computed that avoids the individual storms (modelled as stochastic no-fly zones) and reattaches the original reference trajectory. A case study with a set of simulations is presented herein.

Table of Contents

Executive Summary

Deliverable 4.2 (D4.2) of TBO-Met focuses on Robust Trajectory Planning at tactical level (short-term planning and execution; in this context, between 1 hour and 10 minutes before encountering the convective cells (commonly referred to as storms). This deliverable presents a first step towards the understanding of the inherent uncertainty of storms, and its consideration for the re-routing of aircraft at the tactical level. The uncertain evolution of thunderstorms is considered the only source of uncertainty. We make use of short-term forecasts (also referred to as nowcasts). See TBO-Met's D2.3 Sacher [2] and TBO-Met's D2.4 Sacher and Siegmund [6].

From a methodological point of view, D4.2 includes the following aspects:

- Trajectories calculated using the algorithms presented in D4.1 will be used as input for Task 4.2 (acting as business developed 4D trajectories (BDT)).See TBO-Met's D4.1 in Soler et al. [5].

- Once agreed, the trajectory becomes the Reference Business Trajectory (RBT) to be flown by the airspace user. While the RBT is flown, storms (evolving stochastically) might be encountered and decisions to be taken lay at the tactical level (short-term planning and execution) to ensure safety and at the same time an efficient allocation of resources. The trajectory should be then revised and updated.

- Nowcast information (see TBo-Met's D2.3 Sacher [2] and TBO-Met's D2.4 Sacher and Siegmund [6]) is treated and modelled stochastically (as stochastic storms), and, together with the trajectories in D4.1, incorporated into the DIVMET1 infrastructure for simulation.

- The DIVMET algorithm is used to calculate an updated trajectory (which eventually becomes the revised reference business trajectory (revised RBT) capable of avoiding the storms (modeled as stochastic no-fly zones).

- A set of simulations is conducted in order to estimate the effect of uncertainty on predictability and efficiency of the predicted trajectories under uncertain storms.

D4.2 is structured as follows: We describe the DIVMET algorithm and the modelling of uncertainty in DIVMET in Chapter 2; In Chapter 3 we describe the case studies, including the attained results; finally,

[1] . The DIVMET-Algorithm was initially developed by Thomas Hauf et al [1] at the *Institut für Meteorologie und Klimatologie* of the *Universität Hannover*. It is well described in the PhD thesis of Sakiew [3] and Sauer [4]. In 2014 DIVMET was acquired by MeteoSolutions GmbH and is under further development.

the conclusions are drawn in Chapter 4. In the Appendix, we include a statistical evaluation (provided by AEMET) of the forecast error of nowcast data.

Main results and conclusions that can be drawn include:

- We introduced a methodology for short-term trajectory prediction which is capable of taking uncertainties of thunderstorm cells into account on the tactical planning level (short-term planning and execution). It was found that the methodology is suitable to master the task.
- We derived statistical parameters from the multiple trajectory predictions in order to estimate the effect of uncertainty on predictability and efficiency of the predicted trajectories. The case studies confirmed the working hypothesis that with growing uncertainty the predictability and the efficiency of the predicted trajectories decrease.
- The case studies contained also the comparison of the results between differently effective uncertainty functions. We found here an apparent dependency of predictability and efficiency under the different uncertainty conditions.
- By the detailed analyses of intermediate results of single trajectory predictions we showed that predictability and efficiency are affected strongly by the course of the DBT in context of the adverse weather zone. Additionally, the safety distance that represents the risk awareness of the pilot plays a major role.

All in all, the application of DIVMET algorithm considering uncertainty could be of interest for ATM and may improve the ATM performance in terms of safety, capacity (delays), and environment.

Follow up activities within TBO-Met that are linked with D4.2 include:

- Association to Task 4.3 (and thus D4.3), the validation exercises. Different scenarios will be validated via simulation. The algorithms herein presented will be used to calculate 4D trajectories on tactical level (short-term planning and execution). This will be used as input for WP6.
- Association to WP5, sector capacity analysis. Different 4D trajectories, including its associated uncertainty, will be used as input for the algorithms under development within WP5. The consideration of convection would be herein relevant to plan trajectories that might want to avoid areas of potentially bad weather upon coordination with ATM.

1 Introduction[2]

In the future ATM system, the trajectory becomes the fundamental element of a new set of operating procedures collectively referred to as Trajectory-Based Operations (TBO). Trajectory constitutes a fundamental element of the TBO concept; it is the trajectory that will best meet airline business interests and will evolve out of a collaborative and layered planning process. A major challenge for Trajectory-Based Operations is the existence of significant uncertainties in the models and systems required for trajectory prediction, in particular, thunderstorms. A better understanding of the elements introducing uncertainty in the traffic is key when optimizing, planning, executing, monitoring and synchronizing trajectories with ground systems and/or other aircraft. In TBO-Met, the focus is on Meteorological uncertainty. According to the Grant Agreement [7], meteorological information is provided by Ensemble Prediction Systems (EPS) at the pre-tactical level (mid-term planning) and by EPS and Nowcasts at the tactical level (short-term planning and execution).

According to TBO-Met's Project Management Plan [8], the fundamental goal of WP4 is to analyse trade-offs between efficiency and predictability of 4D trajectories under meteorological uncertainty within the envisioned TBO operational concept. The following sub-objectives arise:

1. Robust trajectory planning at pre-tactical level (mid-term planning: up to three hours before departure) considering wind and convection uncertainty. This is Task 4.1 according to TBO-Met's Project Management Plan [8], which was the aim of deliverable D4.1 (already approved by SJU; see Soler et al. [5]).

2. Improve predictability in trajectory planning at tactical level (short-term planning and execution) considering the uncertainty of individual storm cells within the convective weather regions. This is Task 4.2 according to TBO-Met's Project Management Plan [8], aim of the present Deliverable –D4.2-.

3. The validation via simulation of the above mentioned methodologies. This is partially covered within Task 4.3 according to TBO-Met's Project Management Plan [8], in which a catalogue of simulation scenarios will be produced and included in D4.3. The simulations are part of WP6 according to TBO-Met's Project Management Plan [8].

[2] The opinions expressed herein reflect the author's view only. Under no circumstances shall the SESAR Joint Undertaking be responsible for any use that may be made of the information contained herein.

In other words, we ambition to develop algorithms capable of improving the predictability of aircraft trajectories when subject to meteorological uncertainty, but keeping acceptable levels of efficiency. The following diagram sketches the intended methodologies for WP4.

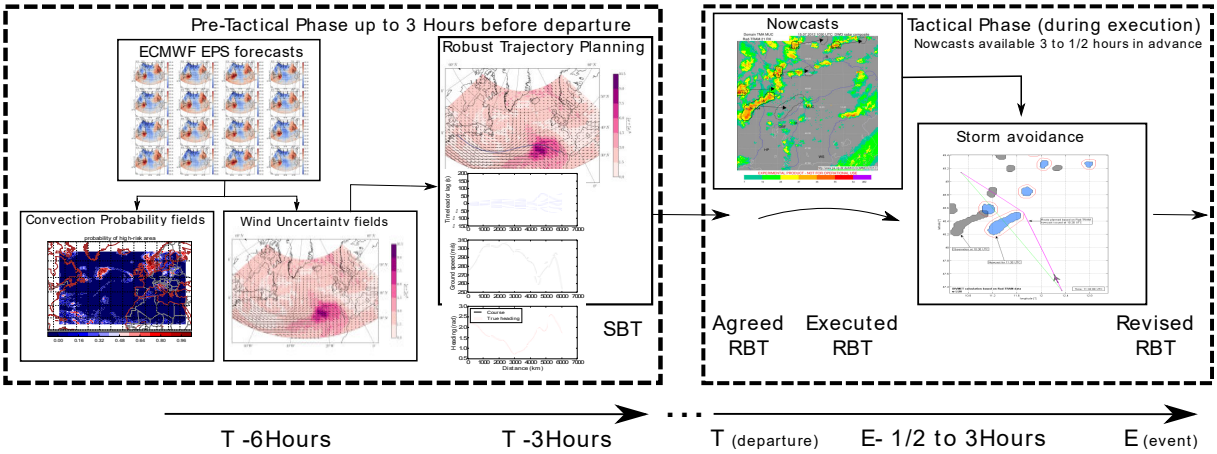

TBO-Met's WP4 Trajectory Planning Methodology for both pre-tactical (mid-term planning) and tactical (short-term planning and execution) levels. Recall that Deliverable 4.2 focuses on the tactical level (right-hand side of the figure)

1.1 Scope of the Deliverable

According to TBO-Met's Project Management Plan [8], the tactical (short-term planning and execution) problem, i.e., right hand side of Figure 1 is subject of study within Deliverable 4.2. Thus, In the present Deliverable we present results on robust trajectory planning at tactical level (short-term planning and execution, in this context around 10 min. to 1 hour before the convective area).

The predictability of the trajectory is subject to uncertainties in location and temporal development of the thunderstorm distribution. It should be noted that for the tactical reaction of A/C to the near future development of storms on the order of several hours the *nowcast* method is applied. Thunderstorm prediction or forecast throughout this paper is understood as nowcasting of storms and is referred to accordingly. However, the terms *storm prediction*, *storm forecast* and *storm nowcast* will be used synonymously.

Supposing the field of high-risk areas would be static in time, the trajectory would also be static and thus highly predictable. That means that due to adverse weather there would be no reason to change the trajectory while the aircraft is following it. At the same time this would be the most efficient and safe route. Thunderstorms however move and develop in time and force pilots to adapt the course accordingly. The predictability of the trajectory depends on the speed and magnitude of the changing adverse weather field and the ability to forecast those changes accurately. One should keep in mind the velocity difference between moving storms and aircraft by a factor of 10. From pilots' perspective while flying around a storm the latter seems to be static. For route planning, even over short times such as 10 minutes storm development cannot be ignored and has to be taken into account. To increase the predictability of trajectories, therefore, one has to use forecasted fields of high-risk areas and to simulate the planned flight through these. DIVMET is capable to do so:

DIVMET performs a dynamic deterministic trajectory prediction according to the field of existing and forecasted high-risk areas. In this context, high-risk areas are defined by the limits of convective cells, typically defined by a prescribed weather radar reflectivity value, e.g. 37 dBZ which are further extended by a safety margin.

The dynamic route planning due to changing weather improves the robustness of the planned route significantly but still is subject to uncertainty related to the forecast quality.

So it is obvious that the predictability of trajectories depends on the quality of the forecast. Using the simplest forecast model, which assumes persistent high-risk areas, the predictability of the trajectory would be low. Assuming a perfect forecast we get a highly predictable trajectory. Reality is somewhere in between these two extremes.

Obviously, the initially planned and adverse weather free route is the most efficient and also most predictable one. In case of adverse weather, the pilot has to navigate around the high-risk areas while at the same time keeping close to the original, most efficient trajectory. The DIVMET algorithm is able to simulate this behaviour and provides (upon user request for any point in space and time) a highly predictable and efficient trajectory to the final destination.

As stated above predictability of trajectories depends on the uncertainty of the adverse weather field. So we have to investigate the related nowcast model uncertainty to find out more about route predictability.

The nowcast data that are used by DIVMET in this project are provided by AEMET. It is described in detail in deliverable D2.3 of TBO-Met (Sacher [2]). The data contains estimates of the location of the centroid of convective cells for the upcoming hour with a time resolution of 10 minutes. Additionally a rectangle encompassing the detected convective cells is provided. Taking this data as input, the software, which was developed in Task 2.4 of TBO_Met (D2.4 Sacher and Siegmund [6]), constructs convective cells with elliptical shape for all lead-times up to one hour.

The authors are fully aware of the restrictions related to considering storms of elliptical shape. This limitation is due to the available data for the project and, however, does not pose a general restriction on the methodology of uncertainty implementation in route planning. State of the art radar storm data consist of gridded weather radar reflectivity fields, which are transformed into polygons of high-risk areas.

To investigate the effect of uncertainty on the trajectory we varied the location of the convective cells randomly within a given range, which is delimited by a defined uncertainty margin. In doing so, we hypothetically assume that those variations are identical with the errors of a typical storm nowcast. The latter was investigated in detail by Manuela Sauer [4] in her PhD thesis, where she also provided numerical values for the forecast error. Among others, we use those values that are described in Section 3.1. DIVMET is applied to each varied adverse weather field resulting in multiple routes. For each route we determine the route length and the related arrival time and compare those values. If the arrival times are close to each other, respectively the dispersion of the arrival time distribution is low, the enforced route deviations are of little impact and the predictability of the arrival times is high. Vice versa, if arrival times are highly scattered, the enforced route deviations have a strong impact. The arrival time distribution may thus serve as a measure of route predictability. Similarly, the route length distribution can be considered as a measure of efficiency. If the enforced deviations do finally

result in more or less equal trajectory lengths, the impact of uncertainty is low. And vice versa, if trajectories differ significantly in length, the uncertainty impact on efficiency can said to be high. However, the ratio of trajectory length and flight time equals the ground speed and is assumed to be constant. Throughout the study we ignore wind effects. Thus mean flight times and arrival time distribution can be converted into each other and there is no need for an extra evaluation of trajectory lengths.

The first objective, therefore, is to determine the mean flight times and the arrival time distribution as a function of uncertainty. This allows us to simply derive at the same time the mean trajectory lengths and length distribution.

As a working hypothesis we assume that flight times and also trajectory lengths grow with growing uncertainty. The question is: are these relations linear or non-linear? From previous work we may conclude that with increasing uncertainty any given storm field may become denser and denser and consequently impermeable. The non-linear nature of this dependency has to be determined quantitatively.

1.2 Acronyms and Terminology

Term	Definition
2D_NAC	Term defines data derived from 2D national radar composite product. NAC is Spanish abbreviation for “nacional”.
A/C	Aircraft
ATC	Air Traffic Control
ATM	Air Traffic Management
BDT	Business Developed Trajectory
NM	Nautical Miles
RADIOE	Effective Radius of a convective cell
RBT	Reference Business Trajectory
SES	Single European Sky
SJU	Sesar Joint Undertaking
TBO	Trajectory-Based Operations
WGS84	World Geodetic System 1984
WP	Work Package

TBO-Met Consortium

AEMET	Agencia Estatal de Meteorología
MetSol	MeteoSolutions GmbH
PLUS	University of Salzburg
UC3M	University Carlos III of Madrid
USE	University of Seville

2 Modelling

2.1 DIVMET

The DIVMET-Algorithm was initially developed by Thomas Hauf et al [1] at the *Institut für Meteorologie und Klimatologie* of the *Universität Hannover*. It is well described in the PhD thesis of Sakiew [3] and Sauer [4]. In 2014 DIVMET was acquired by MeteoSolutions GmbH and is under further development.

Some main features of DIVMET may be enlisted here for better understanding. DIVMET always calculates at a given point in space and time an efficient and safe route to the final destination. For that purpose it also requires an initially planned route as input and furthermore storm data. DIVMET may be operated in various modes.

In real-time simulations, DIVMET determines a route at any instant of time. The route will be recalculated as soon as a weather update occurs and new storm data is provided. Typically, weather radar update times range between 5 minutes minimum and 1 hour maximum, depending on the area.

The route adapts in time steps given by the weather radar availability to the changing weather situation. This simulates the pilot behaviour with the difference that in the simulations the route changes occur at discrete times, while in reality the pilot may change the route continuously, however always in agreement with ATC. Though the route is updated with time, the calculated route assumes a static storm field for the remaining time until the aircraft has landed. The various routes determined during the time of the flight vary strongly with the varying storm field. Thus the predictability of the routes is low.

If with the weather updates also the forecasted weather situation is available, referred to as nowcasts, DIVMET can take those forecasts also into account. For each instant of time, a route simulation will be initiated where the weather nowcasts are used as weather updates along the simulated and forecasted route. The aircraft then moves along that forecasted route. Later occurring necessary changes of the route are only due to forecast errors. The dynamical storm development and the motion of the aircraft with time are well kept by DIVMET.

Nevertheless, the route is of reactive type as it adapts always to the weather situation at each forecast time step and at least in parts resembles a pursuit curve (“dog curve”). A proactive trajectory, in contrast, adapts from the very beginning to a storm position at the time the aircraft would have reached the storm. This proactive route calculation, however, is not yet realized in DIVMET and is mentioned here for reasons of completeness.

A-posteriori simulations are identical with real-time simulations with respect to data flow, as all needed data such as storm observations and nowcasted storms with issuing times and forecast

horizons are stored and available. The major difference is that the real time, often referred to as the wall clock time, is replaced by the simulation time. The progress of the latter depends only on the computing capabilities. These calculations are often referred to as fast time simulations, as e.g. an observed storm case of several hours may be simulated within a couple of minutes.

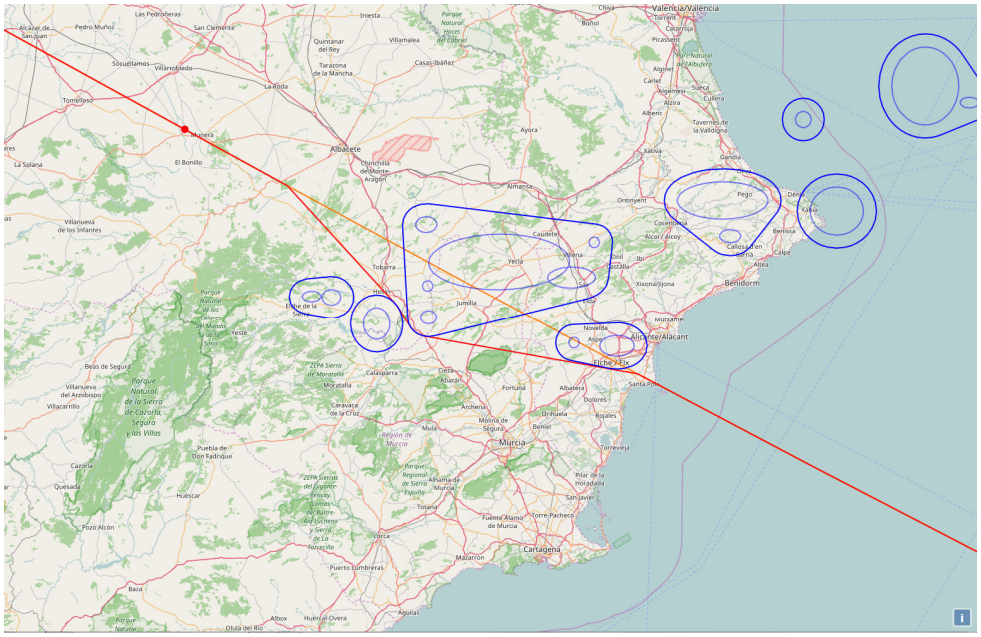

Figure 1: Example of the deviation of convective cells by DIVMET. Red dot marks aircraft position. Orange line shows original trajectory, red line shows deviation. The convective cells (light blue) are surrounded by a safety margin of 5km resulting in a convective hull (dark blue).

2.2 Modelling Uncertainty in DIVMET

In order to consider uncertainty in DIVMET, we do multiple trajectory predictions for each flight while applying minor changes to the field of the high-risk areas. This results in a bunch of trajectories. The trajectories are then analysed according to their flight parameters: track length and arrival time

As described above, DIVMET uses nowcast data for trajectory prediction. Like any forecast, nowcast data exhibits errors which in the context of our studies are considered as uncertainties. A forecast error is simply the difference between the forecasted state and the observed one. As shown in [4] the forecast error is growing with lead-time.

The nowcasts of convective cells was provided by AEMET. The structure and contents of the data was described in detail in deliverable D2.3. Also the data processing to finally delimit high-risk areas as ellipses for lead-times of up to 60 minutes was described in deliverable D2.3 (Sacher [2]). These high-risk areas should not be crossed by any aircraft.

In the context of this study a storm is described by a column of elliptical base. Here we spatially consider the problem in 2-D only. We consider as uncertainty parameter the location of the centroid. As the data does not provide information on development or decay of the nowcasted thunderstorm

orientation and area of the ellipse, which would also be uncertain, these parameters are not examined. We further assume that all ellipses across the variations are geometrical similar with an identical semi axes ratio. This assumption is in line with the above-mentioned crude approximation of storm shape by an ellipse.

In order to model uncertainty in DIVMET, we varied stochastically the location of the centroid by the scale of the typical displacement errors for the respective lead-times. That means that with growing lead-time and thus growing displacement error the variation range of the location is growing too. This is illustrated in Figure 2 and Figure 3. The displacement error is modelled as an uncertainty margin around the originally forecasted cell. This is also described in detail in Deliverable D2.3 (Sacher [2]).

The varied high-risk areas are additionally surrounded by a safety margin. The magnitude for both margins is configurable by the user of DIVMET.

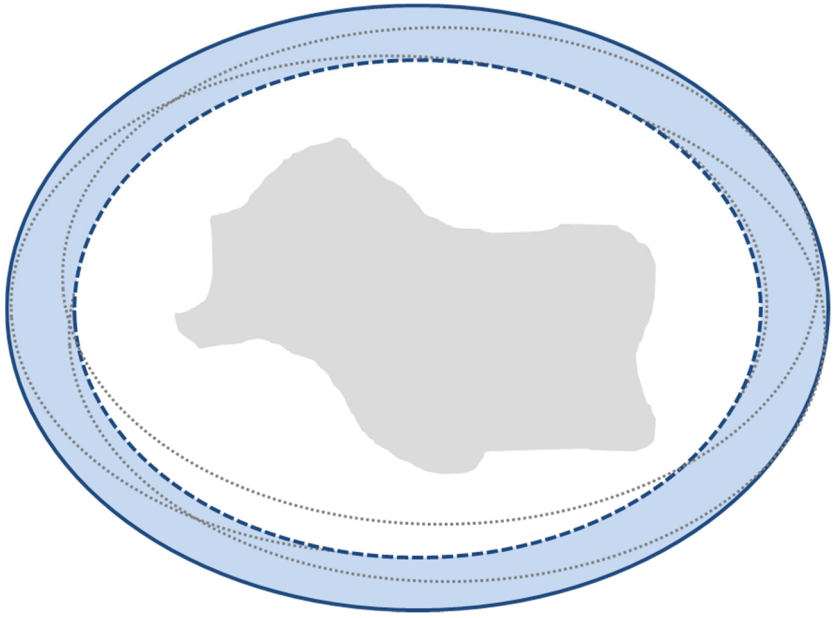

Figure 2: Illustration of the variation of the ellipses (dotted grey) within a small uncertainty margin (light blue area) for a low lead-time. Original ellipse from the input data is dashed blue. Shape of the original storm is filled in grey.

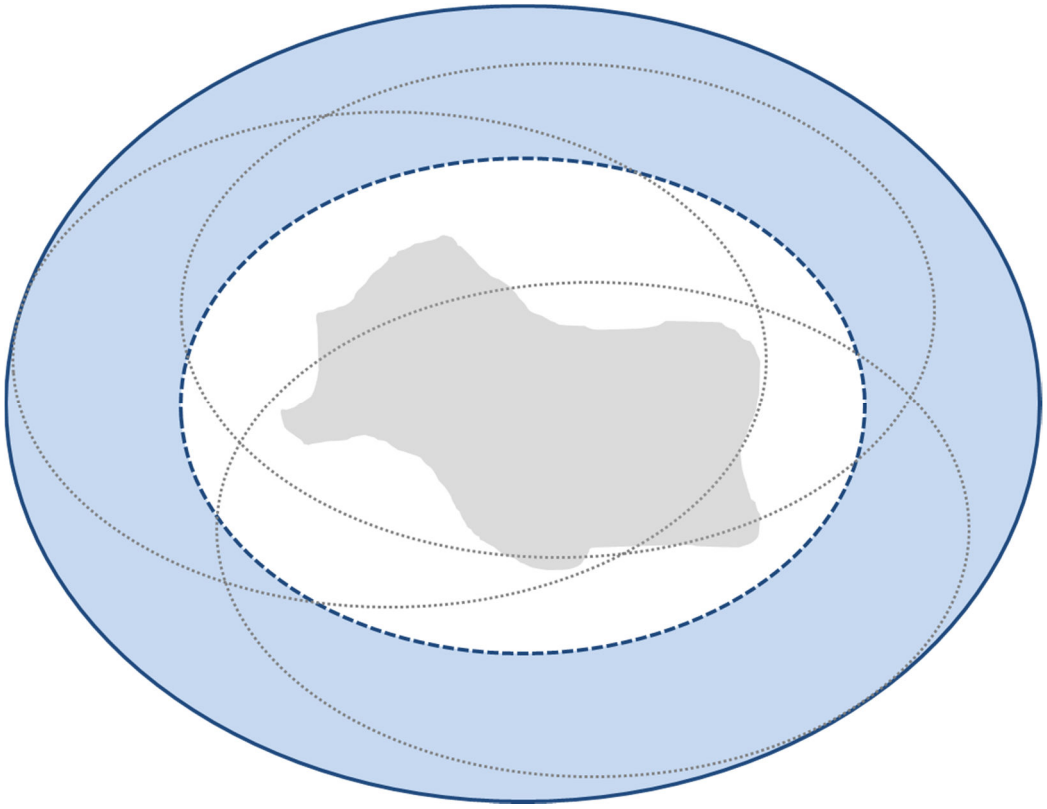

Figure 3: Illustration of the variation of the ellipses (dotted grey) within a big uncertainty margin (light blue area) for a high lead-time. Original ellipse from the input data is dashed blue. Shape of the original storm is filled in grey.

For further studies in the scope of this task we aim to vary the ellipse's orientation and area stochastically within the uncertainty margin. We prescribe the size of the uncertainty margin (area filled in light blue in Figure 2 and Figure 3) and vary position stochastically but such that the resulting ellipses are still bounded by the uncertainty margin. Note that the uncertainty may also lead to smaller distances to the original storm (grey filled inner area in Figure 2 and Figure 3)

3 Case Study

With the case studies we aim to examine the effects of uncertainty on predictability and efficiency of 4D trajectories on the tactical level as outlined above.

We simulate several flights (input from D4.1, see Soler et al. [5].) under adverse weather conditions by varying the uncertainty of thunderstorms, which we include intoDIVMET. We use five different lead-time dependent functions, which give uncertainty margins. Among these, one function based on the results found by Sauer [4] and one based on the evaluation of the 2D_NAC data by AEMET (please, refer to the Appendix). All functions are monotonically increasing with lead-time. In case of function F3 by Sauer [4] the uncertainty margin grows with lead-time from approx. 1.5 km to 20 km for 10 minutes and 60 minutes, respectively. The functions are described in Section 3.1.

In Section 3.2 we apply DIVMET on three different routes, using an ensemble of different nowcast datasets for the same period of time. So we get a trajectory prediction for each ensemble member.

The trajectories are analysed in Section 3.3 in order to find principles in how tactical trajectory prediction is affected by uncertainties in nowcasts. For this we used frequency distributions of arrival time delays and derived statistical parameters from these (Section 3.3.1). Additionally we examined the trajectory prediction process through the nowcast steps for all lead-times from 0 to 60 minutes (Sections 3.3.2 and 3.3.3).

3.1 Varying Nowcasts by Uncertainty

We use five different functions to model the lead-time dependent uncertainty margin:

$$f(\tau) = a_2\tau^2 + a_1\tau + a_0$$

F1: coefficients $a_2 = 0, a_1 = 0.25, a_0 = 0$

F2: coefficients $a_2 = 0, a_1 = 0.5, a_0 = 0$

F3: coefficients $a_2 = 0, a_1 = 0.75, a_0 = 0$

F4: coefficients $a_2 = -0.002, a_1 = 0.4336, a_0 = 1.6721$ (as found by Sauer [4])

F5: $f(\tau) = 0.052\tau^{1.56}$ (based on the analysis included in the Appendix)

The resulting uncertainty margins from equations F1 to F5 are in kilometres. The lead-time τ is given in minutes.

Functions F1 to F5 are shown in Figure 4.

Function F5 is derived from the results of a study performed by AEMET (please, refer to the analysis included in the Appendix). AEMET statistically evaluated the forecast error of the nowcast data provided to this project. These results are shown in Figure 4 as circles. The fitted function F5 is described as a magenta coloured line.

As described in Section 2.2, the forecasted convective cells are randomly varied in location using a Gaussian probability density function within the limits of these functions in respect of the lead-time.

So we get a set of forecast variations $V_0, \ldots, V_M$ for each uncertainty margin function. One set of forecast variations is comprised of M runs with stochastically varying position of the storm ellipse bounded by the prescribed uncertainty margin. With five sets (F1, …, F5) we have an artificially created weather data basis for 5 times M DIVMET simulations (trajectory predictions) of one input trajectory.

As a number for M we chose 30. This order is determined empirically and is considered to be a good compromise between statistical significance and computing time.

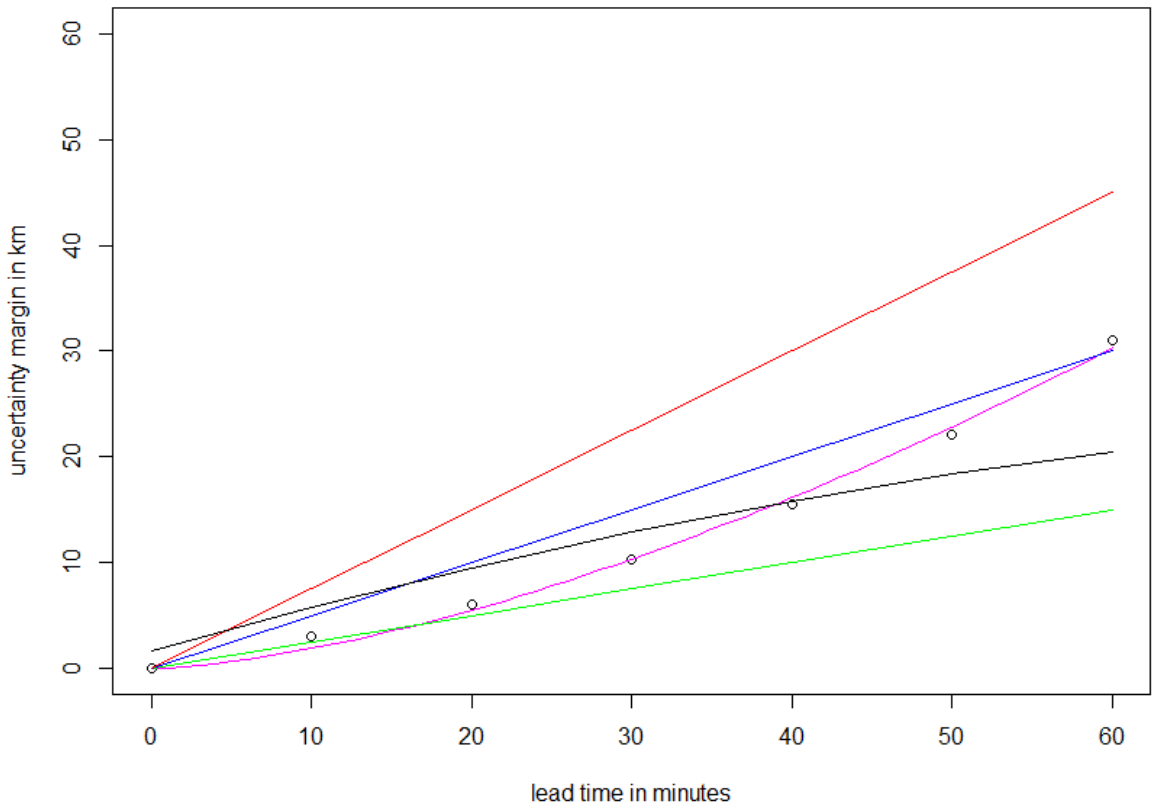

Figure 4: This figure shows the five functions which are used to quantify the uncertainty margin as a function of lead-time: F1 (green), F2 (blue), F3 (red), F4 (black) and F5 (magenta).

3.2 DIVMET Simulations

For each set of varied forecasts we simulated trajectory predictions with DIVMET software.

The software used different configurations for the safety margin: 5NM, 10NM. As maximum angles at leave and re-join point of the deviation from the original route 35° were allowed.

As initial flight routes we used three trajectories which were simulated in Task 4.1 and included in D4.1 (see Soler et al. [3]; Chapter 6).. These are three different BDT from strategic planning stage for a flight that departs from New York with destination Alger at 2016/12/19, 3:00. The DIVMET simulation starts on waypoints about one hour before arrival. For route R1 this is waypoint (40.177N, -5.184E) at 2016/12/19, 8:32. The routes cross an area of convective storms on the east coast of Spain. Speeds are considered to be constant and equal to M0.82.

The three BDTs are identified by:

Route R1: 1_TBOmet_20161219_0900_ecmf_cp0_dp0[3]

Route R2: 1_TBOmet_20161219_0900_ecmf_cp0.001_dp0

Route R3: 1_TBOmet_20161219_0900_ecmf_cp0.009_dp0

For further details on the routes refer to Section 3.3.1.

The processing of the DIVMET simulation of one flight is as follows:

DIVMET initially takes the BDT as input and calculates the first deviation route, taking into account all available nowcasts. The airplane then is virtually moved along the deviation route according to the forecast lead-times (see Figure 5). This results in the RBT at the initial real aircraft position. In order to calculate the next trajectory for the airplane on its way to the destination airport, the aircraft is moved along this RBT resulting in a new real aircraft position (10 minutes later). Now DIVMET takes this RBT as input (assuming that the pilot is accepting the deviation proposal from DIVMET) and calculates a new RBT considering a nowcast update (see Figure 6). This procedure will be repeated until the aircraft reaches the destination.

DIVMET puts out one RBT for each real aircraft position, e.g. 8:32, 8:42, 8:52,… 9:32

For each uncertainty margin function (F1… F5) there are approximately[4] 210 RBTs.

[3] The nomenclature is as follows: 20161219 (date); 0900 (9 hours time step; notice that the forecast is produced at 00.00); ecmf (source of data; EPS from the European Center of Medium-Range Weather Forecast); cp0 (convective penalty equal to 0, as in D4.1); dp0 (dispersion penalty equal to 0, as in D4.1).

[4] It is due to the development stage of the DIVMET algorithm that this number cannot be given exactly. Not every DIVMET run succeeds in a valid response. For a minor number of situations it is possible that the algorithm does not find a solution.

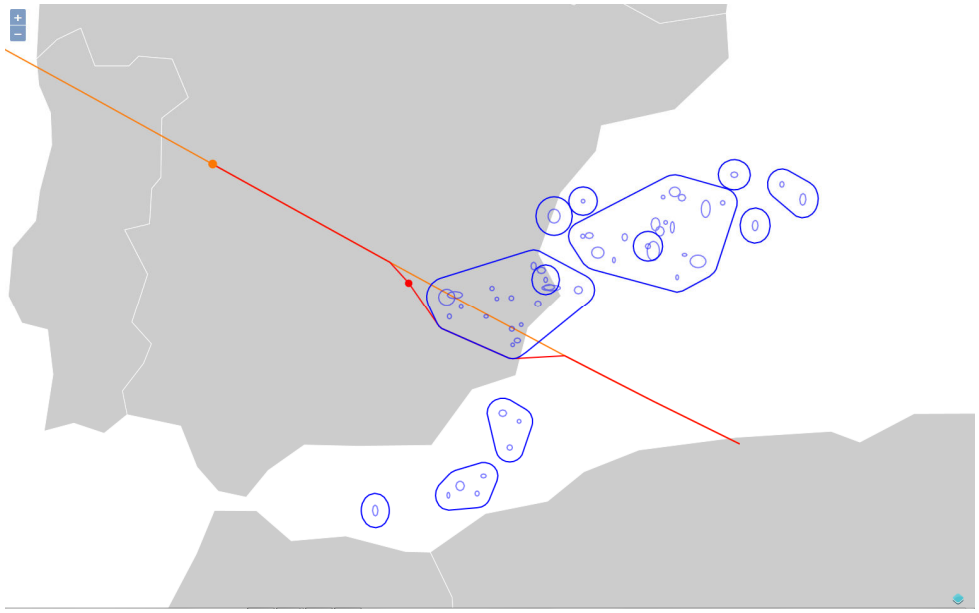

Figure 5: DIVMET simulation area for the analysed flight at 2016/12/19, 8:32. The orange dot marks the real position of the aircraft. The red dot marks the virtual position of the aircraft at 24 minutes forecast lead-time. The orange line is the BDT, the red line is the RBT calculated by DIVMET. Shown here is route R1.

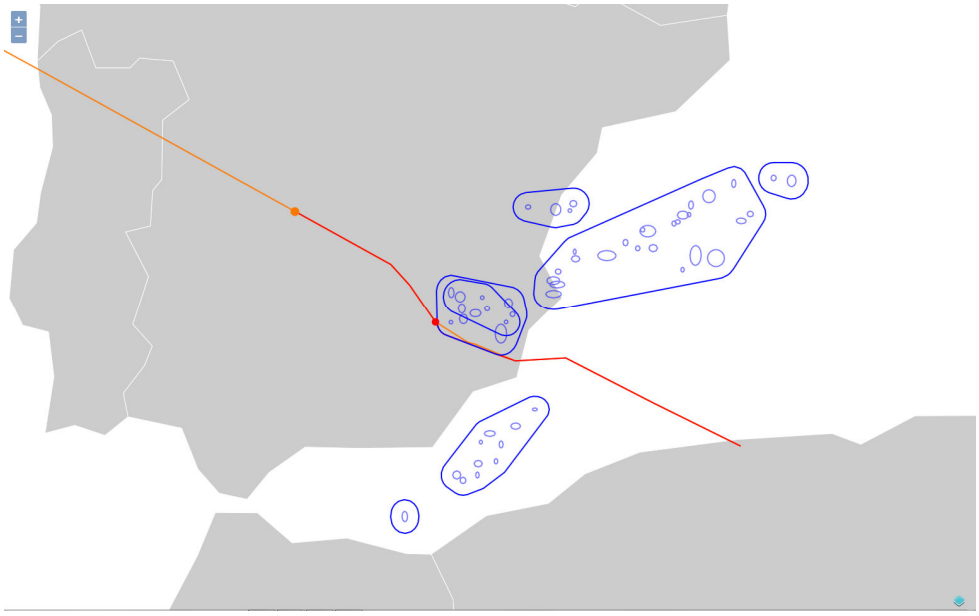

Figure 6: DIVMET simulation for the analysed flight at 2016/12/19, 8:42. One time step later than Figure 5. The orange dot marks the real position of the aircraft. The red dot marks the virtual position of the aircraft at 19 minutes forecast lead-time. The orange line to the aircraft position is still the BDT, followed by the RBT form the last DIVMET result. This is input to the newly calculated RBT by DIVMET. Shown here is route R1.

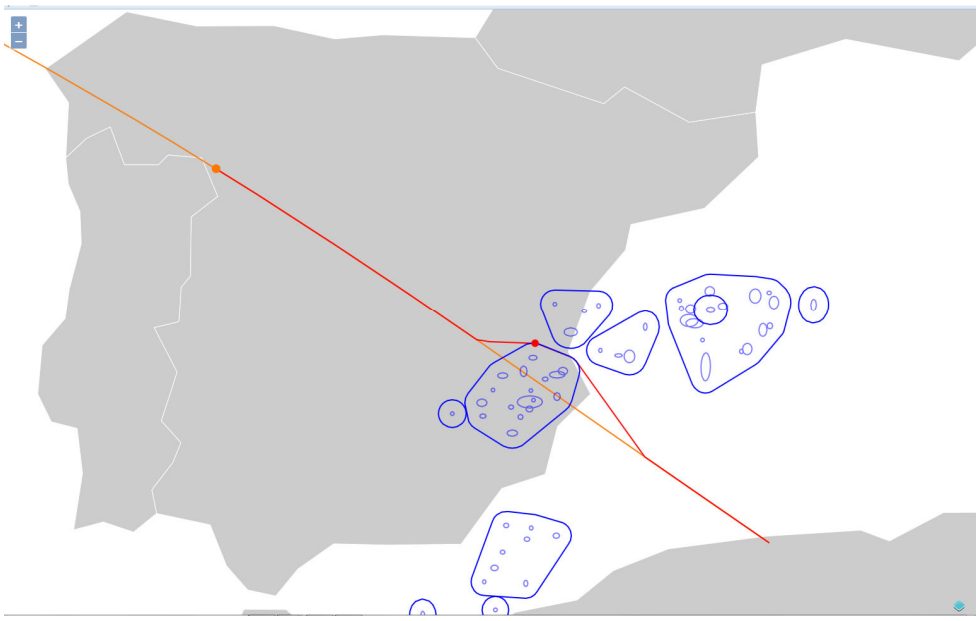

Figure 7: DIVMET simulation for the analysed flight at 2016/12/19, 8:25. The orange dot marks the real position of the aircraft. The red dot marks the virtual position of the aircraft at 39 minutes forecast lead-time. The orange line to the aircraft position is still the BDT, followed by the RBT form the last DIVMET result. This is input to the newly calculated RBT by DIVMET. Shown here is route R2.

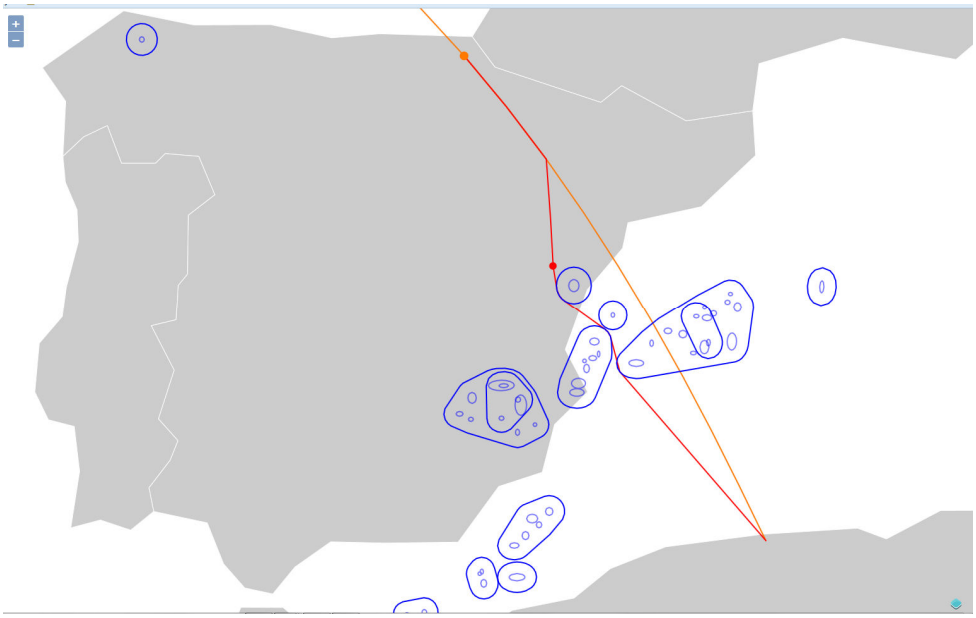

Figure 8: DIVMET simulation for the analysed flight at 2016/12/19, 8:57. The orange dot marks the real position of the aircraft. The red dot marks the virtual position of the aircraft at 24 minutes forecast lead-time. The orange line to the aircraft position is still the BDT, followed by the RBT form the last DIVMET result. This is input to the newly calculated RBT by DIVMET. Shown here is route R3.

3.3 Analyses of DIVMET Simulations

The simulations in Section 3.2 offer a big pool of DIVMET responses and intermediate results which will be examined in this section.

As DIVMET response (RBT) we call the final result, i.e. the predicted trajectory for one instance of time that takes all available nowcasts into account.

As intermediate result we call a predicted trajectory for one instance of time that is calculated up to a certain forecast lead-time. So the last intermediate result is the DIVMET response.

3.3.1 Frequency Distributions of arrival time delays

In this section we examine DIVMET responses of route R1 which are calculated under different uncertainty conditions F1… F5. As mentioned above we provided 30 different variations V_1…V_{30} of weather objects for each uncertainty condition. This results in about 180 RBTs throughout the one hour flight until arrival (about 6 RBTs considering weather updates every 10 minutes). The simulations are run with a safety margin of 10NM.

Figure 9 through Figure 13 show the frequency distributions of the arrival time delays based on the initially planned BDT. The abscissa shows arrival time delays in s with class width of 10 s. The ordinate is normalised by the number of DIVMET responses.

In order to evaluate the calculated statistical moments (mean and standard deviation) a Gaussian probability density function is added to the frequency distribution.

In this study delay is calculated by using RBT at lead-time τ_N by using:

$$\Delta_k = \left(t_{RBT,k} - t_{DBT}\right)$$

Mean delay is calculated by using:

$$\mu = \frac{1}{M}\sum_{k=1}^{M}(\Delta_k)$$

Standard deviation is calculated by using:

$$\sigma = \sqrt{\frac{1}{M}\sum_{k=1}^{M}(\Delta_k - \mu)^2}$$

Dispersion is calculated in terms of the spread:

$$\delta = \max\left(t_{RBT,1}, \dots, t_{RBT,M}\right) - \min\left(t_{RBT,1}, \dots, t_{RBT,M}\right)$$

with

M: Number of variations V_1…V_M, $M=30$

N: Number of forecast lead-times.

$t_{RBT,k}$: Arrival time of Reference Business Trajectory (RBT) under variation V_k at lead-time τ_N

t_{DBT}: Arrival time of Developed Business Trajectory DBT

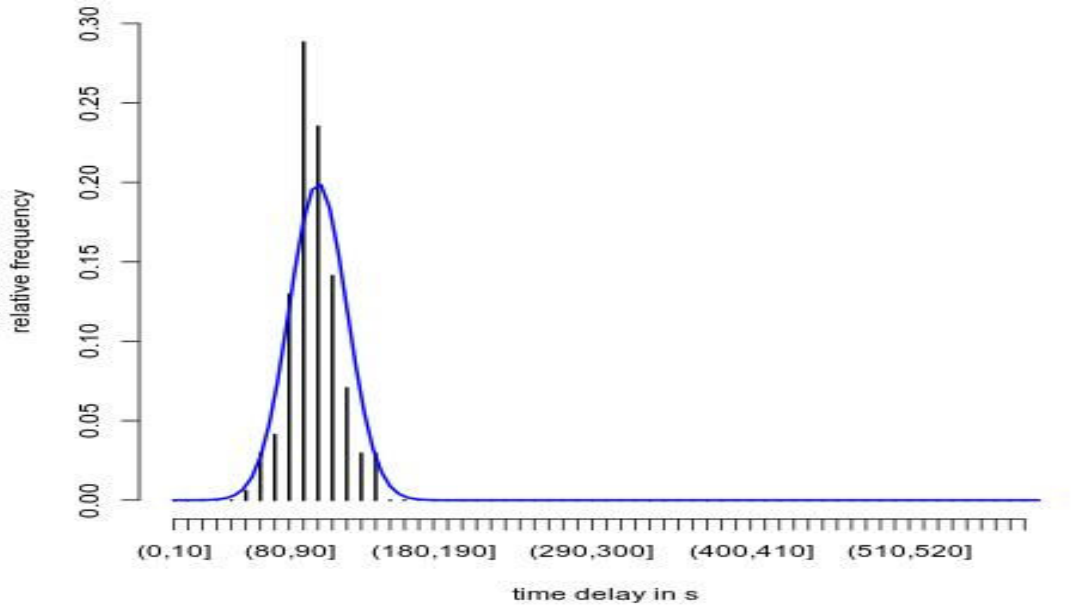

Figure 9: Frequency distribution of arrival time delays for route R1 under uncertainty condition F1 ($f(\tau) = 0.25\tau$). Abscissa shows arrival time delays in s with class width of 10 s. The blue line is a fitted Gaussian probability density function. Safety distance: 10NM.

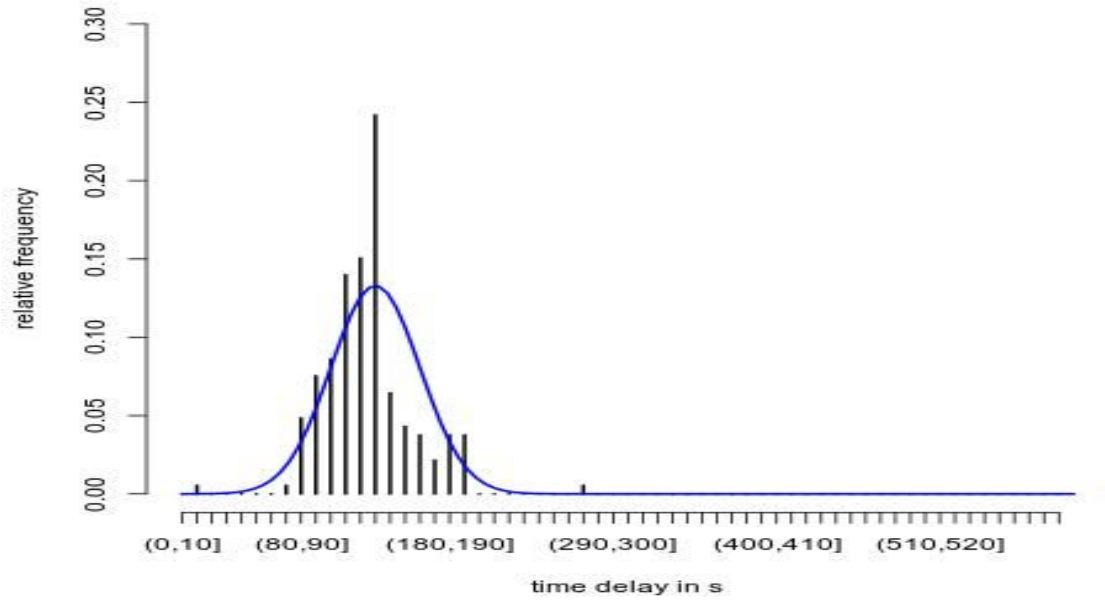

Figure 10: Frequency distribution of arrival time delays for route R1 under uncertainty condition F2 ($f(\tau) = 0.5\tau$). Abscissa shows arrival times in s with class width of 10 s. The blue line is a fitted Gaussian probability density function. Safety distance: 10NM.

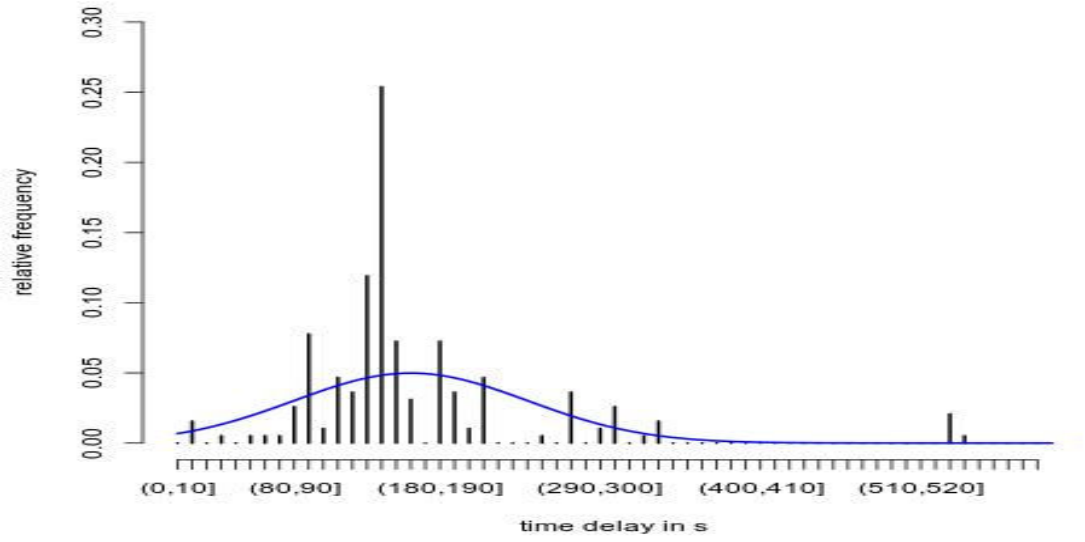

Figure 11: Frequency distribution of arrival time delays for route R1 under uncertainty condition F3 ($f(\tau) = 0.75\tau$). Abscissa shows arrival time delays in s with class width of 10 s. The blue line is a fitted Gaussian probability density function. Safety distance: 10NM.

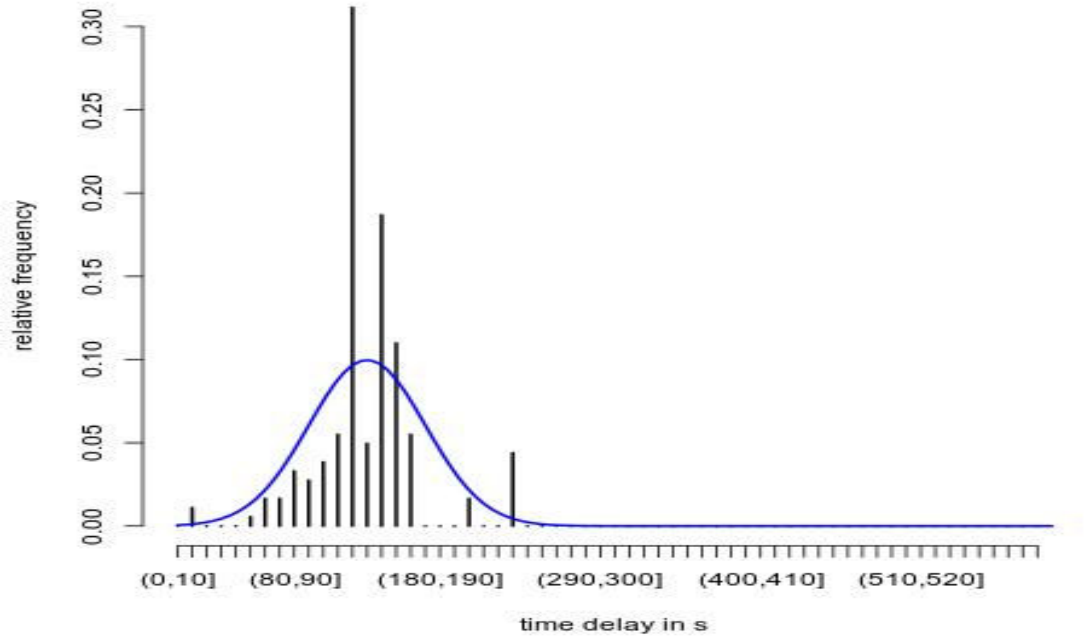

Figure 12: Frequency distribution of arrival time delays for route R1 under uncertainty condition F4 ($f(\tau)$, Sauer). Abscissa shows arrival times in s with class width of 10 s. The blue line is a fitted Gaussian probability density function. Safety distance: 10NM.

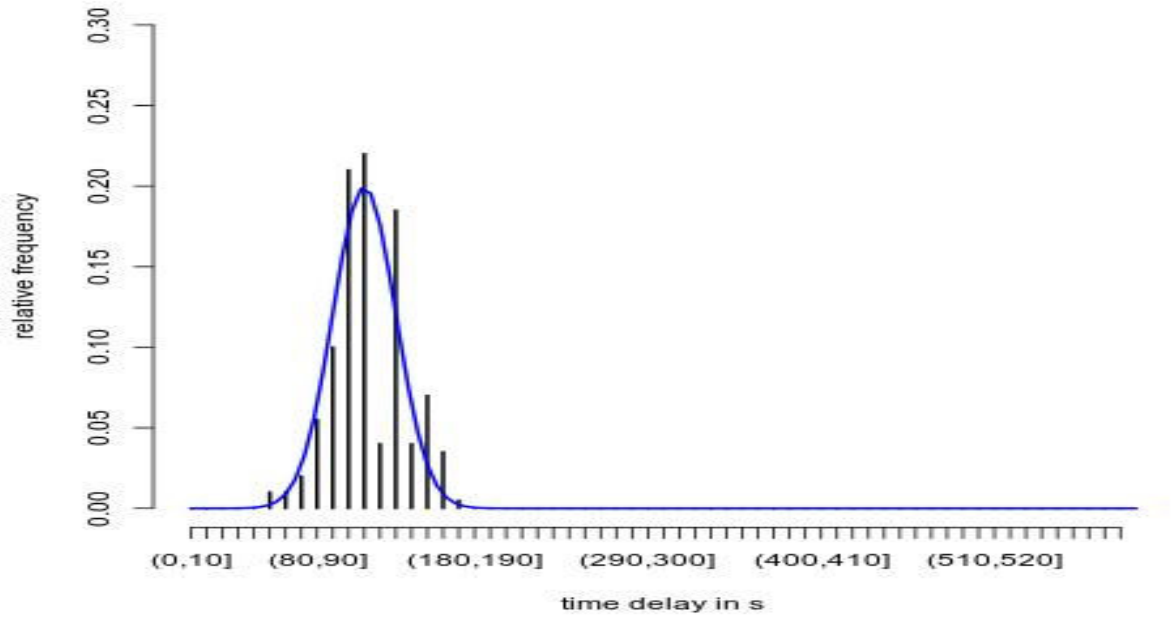

Figure 13: Frequency distribution of arrival time delays for route R1 under uncertainty condition F5 ($f(\tau)$, AEMET). Abscissa shows arrival times in s with class width of 10 s. The blue line is a fitted Gaussian probability density function. Safety distance: 10NM.

	Mean delay [s]	Standard deviation [s]	Spread [s]
F1	102	16	89
F2	130	30	260
F3	167	84	526
F4	133	34	218
F5	117	22	119

Table 1: Overview of statistical parameters derived from the analysis of the simulations with 10NM safety margin. Route R1.

The frequency distributions in Figure 9 through Figure 13 and the statistical parameters in Table 1 show the expected results. Regarding uncertainty conditions F1…F3, mean delay, standard deviation of delay and spread of delay grow with increasing uncertainty. While the mean only differs 60s between F1 and F3, the frequency distribution widens significantly with a difference in standard deviation of 68s and a spread of 526s for F3 and 89s for F1.

Uncertainty functions F4 and F5 run between F1 und F2. Although F4 crosses F5 at about 40 minutes of forecast lead-time and the functional values of F5 are 5km and 10km higher at 50 and 60 minutes compared to F4, the smaller values of F5 in the range of 0 to 30 minutes result overall in smaller values of the statistical parameters. This may lead to the assumption that uncertainties at lower lead-times affect the tactical rerouting more than uncertainties at higher lead-times. This is examined in Section 3.3.2.

Analyses of auxiliary Routes

The above analysis was applied to the results of the simulations of two other routes, R2 and R3. For these routes the results of the simulations under uncertainty conditions F5 are further commented in this deliverable.

As displayed in Figure 7 and Figure 8 the BDT of routes R2 and R3 are planned to cross the convective area more north-easterly than route R1, with R3 being outmost. In contrast to R1, routes R2 and R3 are facing a convective area with a wide lateral extend in both port and starboard direction. Under these conditions and with regard to rerouting in DIVMET we suppose that the probability of broader deviations is high. This may result in longer tracks and on the average in bigger mean delay. The statistic results do not confirm this hypothesis in general. Looking at the frequency distributions in Figure 14-15, we see that the distributions are not Gaussian. Especially Figure 14 shows two maxima. In addition the mean to median value difference for R2 and R3 is significant, being very low for R1 at the same time. The two maxima can be interpreted as two major tracks that are being suggested by the DIVMET algorithm. The uncertainty variations are cause for the spreading of the tracks' delays around the maxima. In Figure 15, the maxima are not so distinct but still can be indicated.

In Table 2, an overview of the statistical parameters derived from the analysis of the simulations with 10NM safety margin is presented.

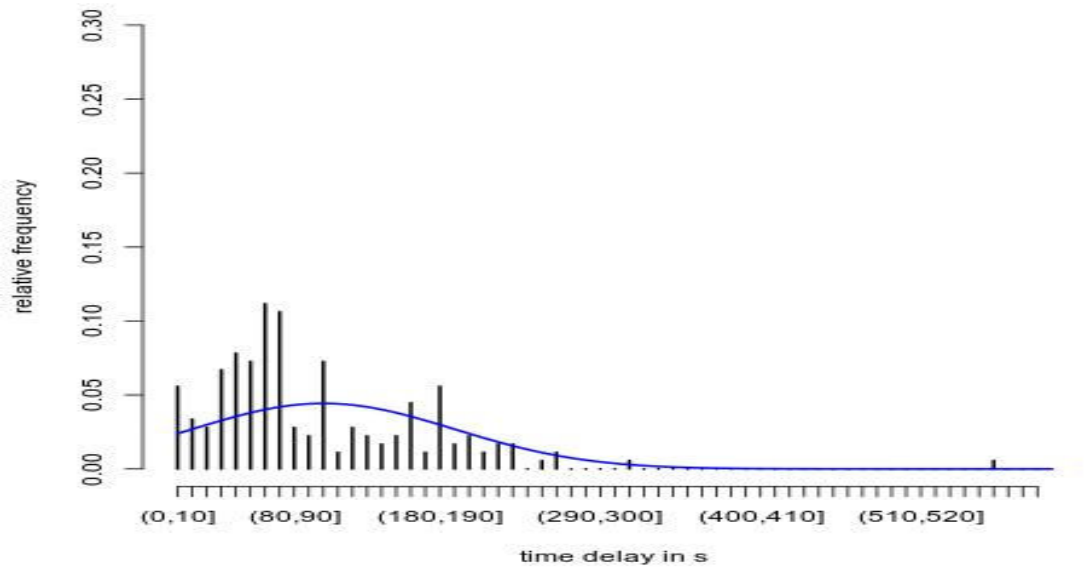

Figure 14: Frequency distribution of arrival time delays for route R2 under uncertainty condition F5 ($f(\tau)$, AEMET). Abscissa shows arrival times in s with class width of 10 s. The blue line is a fitted Gaussian probability density function. Safety distance: 10NM.

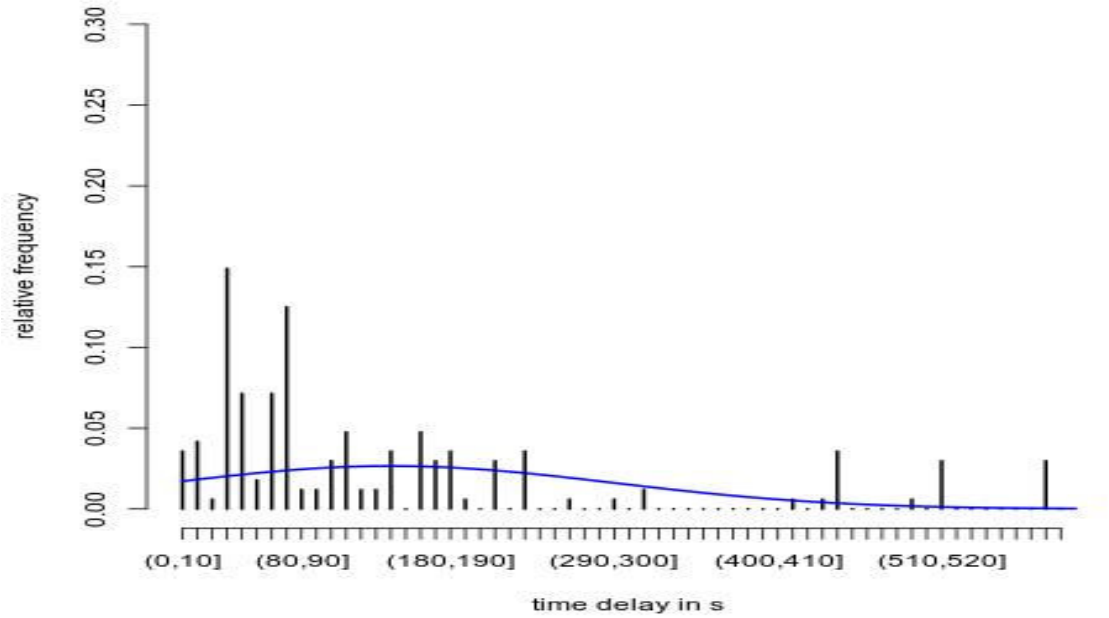

Figure 15: Frequency distribution of arrival time delays for route R3 under uncertainty condition F5 ($f(\tau)$, AEMET). Abscissa shows arrival times in s with class width of 10 s. The blue line is a fitted Gaussian probability density function. Safety distance: 10NM.

	Mean [s]	Standard deviation [s]	Spread [s]
R1	117	22	119
R2	102	89	744
R3	145	149	594

Table 2: Overview of statistical parameters derived from the analysis of the simulations with 10NM safety margin. Comparison of different routes R1, R2 and R3 using uncertainty conditions F5.

Reduction of the Safety Margin

The three routes were simulated with DIVMET by using a smaller safety margin. The safety margin is always put around the convective cells. As uncertainty conditions for the simulations function F5 (AEMET) is used. The statistical parameters of the delays of the trajectory bundle confirm the hypothesis that with smaller extend of the convective areas the deviated tracks become shorter. The length of rerouted R3 tracks decrease very strongly from an average of 145s (10NM safety margin) to 13s (5NM safety margin). This is due to the fact that convective cells with higher safety margin merge to bigger connected convective areas whereas smaller safety margins tend to produce scattered fields of convective cells. DIVMET then navigates the A/C around these smaller shapes. With bigger safety margin the then connected and merged convective cells bigger shapes which have to be navigated around in a broader manner. An extreme example is shown in Figure 16.

In Table 3, an overview of the statistical parameters derived from the analysis of the simulations with 5NM safety margin is presented.

	Mean [s]	Standard deviation [s]	Spread [s]
R1	74	15	82
R2	70	96	475
R3	13	11	38

Table 3: Overview of statistical parameters derived from the analysis of the simulations with 5NM safety margin. Comparison of different routes R1, R2 and R3 using uncertainty conditions F5.

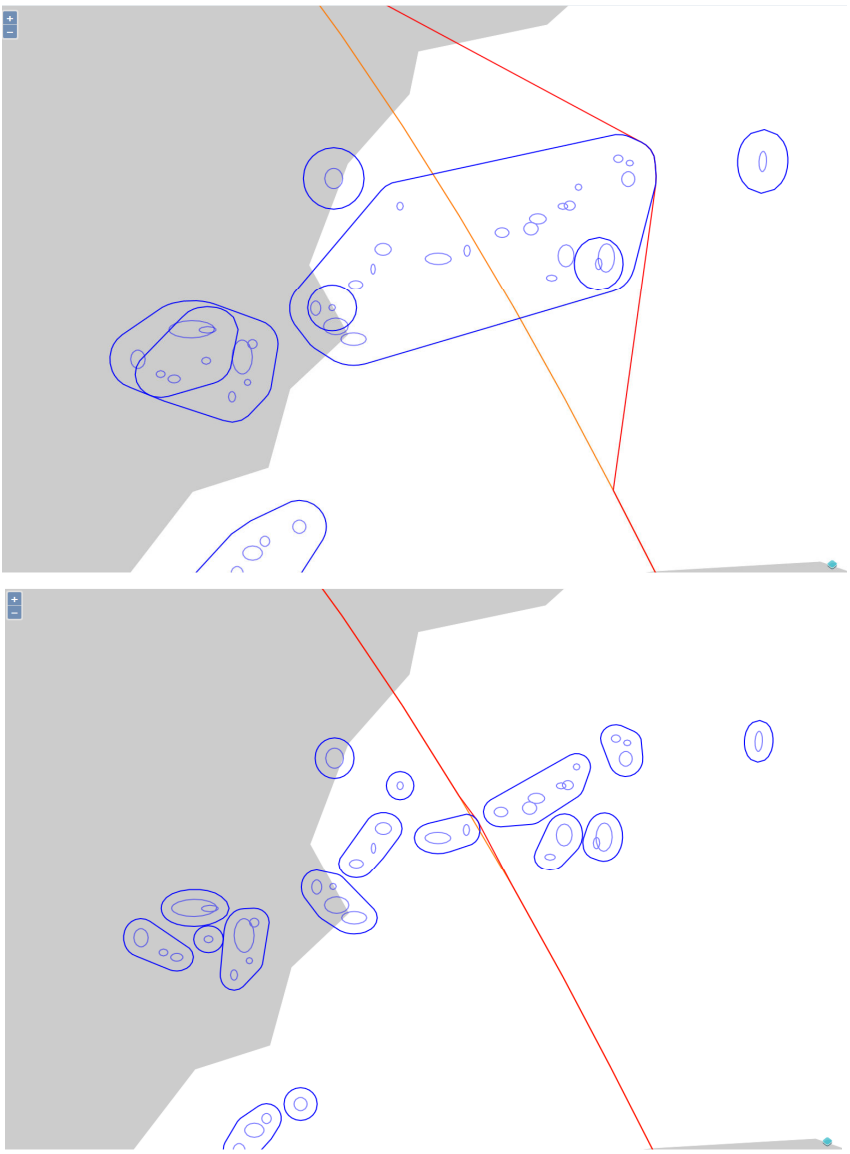

Figure 16: Extreme example for the dependency of the trajectory prediction on safety margin. Above with safety margin of 10NM and below 5NM.

3.3.2 Comparison using different uncertainty/lead-time functions

With the help of the intermediate results of DIVMET, we investigate the predictability and efficiency of the predicted trajectories while stepping through the nowcasts up to 1 hour of lead-time.

Again we have 30 different variations $V_1 \ldots V_{30}$ of weather objects for each uncertainty condition F1…F5. This results in 30 RBTs for each forecast lead-time. The simulations are run with a safety margin of 10NM.

The equations to calculate the statistical parameters are basically the same as in Section 3.3.1, but the parameters are calculated independently for each lead-time.

Delay is calculated independently for each lead-time $\tau_1 \dots \tau_N$ by using:

$$\Delta_{k,\tau} = \left(t_{RBT,k,\tau} - t_{DBT}\right)$$

Mean delay is calculated by using:

$$\mu_\tau = \frac{1}{M} \sum_{k=1}^{M} \left(\Delta_{k,\tau}\right)$$

Standard deviation is calculated by using:

$$\sigma_\tau = \sqrt{\frac{1}{M} \sum_{k=1}^{M} \left(\Delta_{k,\tau} - \mu_\tau\right)^2}$$

The spread is now calculated independently for each lead-time $\tau_1 \dots \tau_N$ by using:

$$\delta_\tau = \max\left(t_{RBT,1}, \dots, t_{RBT,M}\right) - \min\left(t_{RBT,1}, \dots, t_{RBT,M}\right)$$

with

M:	number of variations $V_1 \dots V_M$, $M=30$
$t_{RBT,k,\tau}$:	arrival time of intermediate Reference Business Trajectory under variation V_k at forecast lead-time τ
t_{DBT}:	arrival time of Developed Business Trajectory

Here we present the results of the analyses of the predicted trajectories based on route R1. The real position of the A/C is on waypoint (40.177N, -5.184E) at 2016/12/19, 8:32. The A/C is moved virtually along the predicted trajectory, which is updated every lead-time step of 5 minutes. For each lead-time we get 30 predicted trajectories.

Figure 17 shows the mean delay over forecast lead-time for the 30 different trajectory predictions of route R1 and under different uncertainty conditions F1…F5. Additionally the results of the trajectory simulated without uncertainty is displayed as a reference. As described above, mean delay is an inverse measure of efficiency as we do not consider wind here. Comparing the lines connected to the uncertainty functions F1…F5 with the line without uncertainty, it can be seen that any uncertainty, which is inputted into the trajectory prediction algorithm, will result in an increase of the mean delay. That means that efficiency is decreasing. While the lines stay close together up to ten minutes of lead-time, the spread increases fast up to 40 minutes and then staying constant. The constant level from 40 to 60 minutes is due to the fact that the A/C has virtually passed the area of convective activity and has no further cells ahead, so that the predicted trajectory does not change anymore.

In general results show the expected flow. The delays stay mostly inside the hull that is given by the lines of the least and the most effective uncertainty function F1 and F3, with maximum delays of 87s and 125s, respectively.

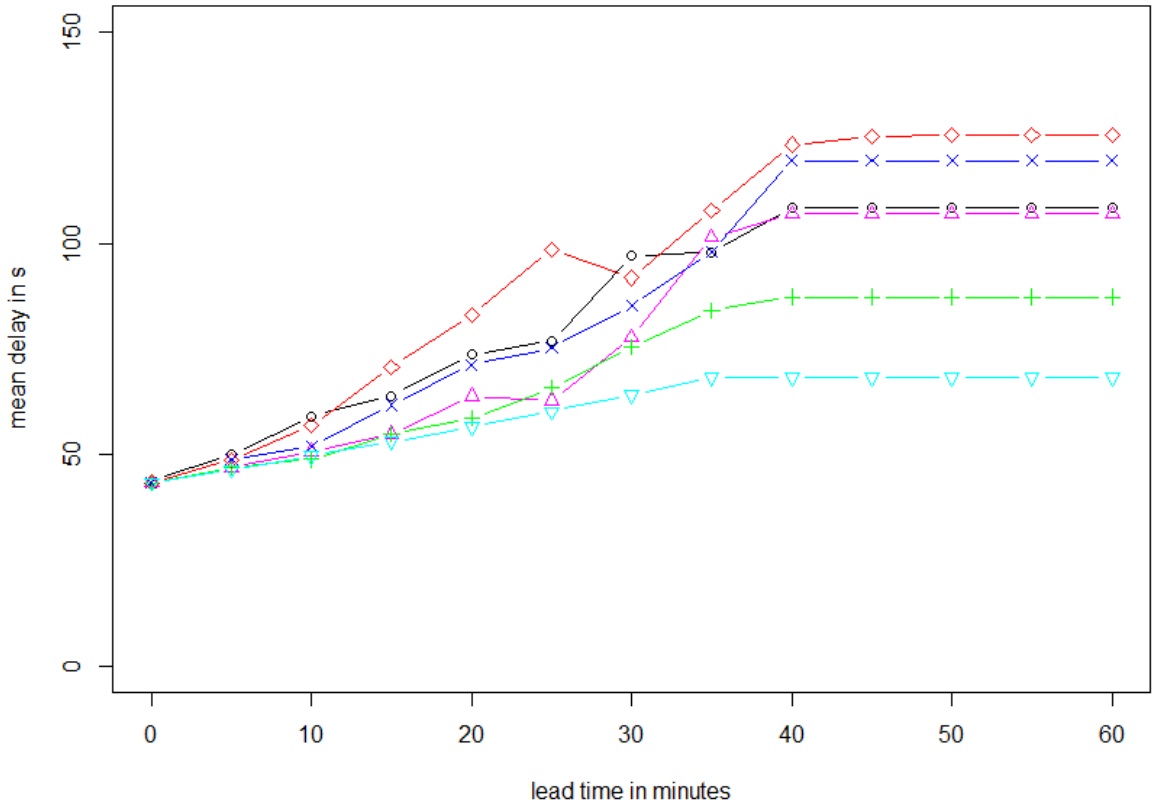

Figure 17: Mean Delay over forecast lead-time for route R1 with different uncertainty margin functions: F1 (green), F2 (blue), F3 (red), F4 (black), F5 (magenta) and no uncertainty (cyan).

Figure 18 shows the dispersion (spread) over forecast lead-time for the 30 different trajectory predictions of route R1 under different uncertainty conditions F1…F5. As described above, dispersion is an inverse measure of predictability of the predicted trajectories. That means that a low dispersion among predicted trajectories can be viewed as high predictability. It is expected dispersion to increase with growing uncertainty. As uncertainty increases with growing lead-time, the dispersion lines in Figure 18 show this. Again the lines spread significantly with growing lead-time. It is noted that all lines show a local maximum between 25 and 30minutes of lead-time. We identified that this lead-time range correspond to the area of convective activity. That means that the A/C deviates virtually around the convective area in this lead-time range. The local maxima are caused by small range tactical manoeuvres while closely facing the convective cells. Once a deviation trajectory is determined and followed by the A/C the reactions to the next forecast do not have to be as strong as before or the route can even be optimized, which results in the decay of the lines of F1, F2 and F5 following the local maximum.

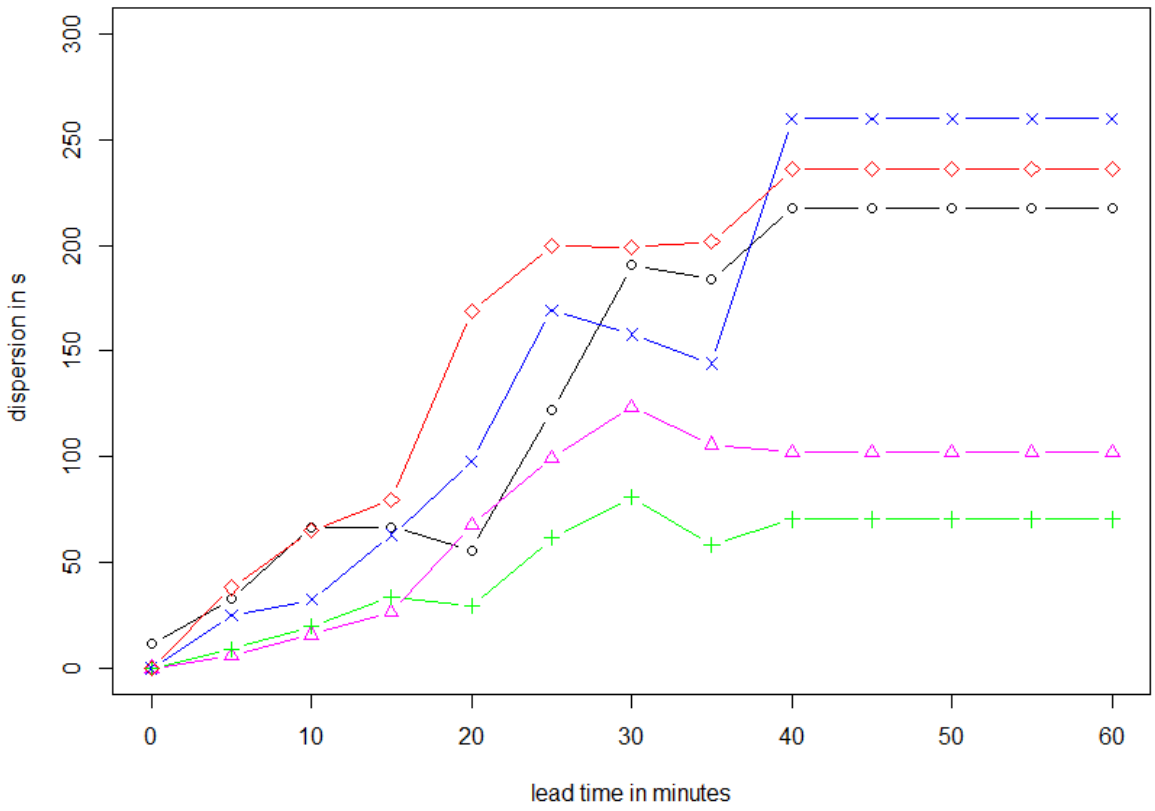

Figure 18: Dispersion (spread) over forecast lead-time for route R1 with different uncertainty margin functions: F1 (green), F2 (blue), F3 (red), F4 (black) and F5 (magenta).

3.3.3 Comparison of different routes using one uncertainty/lead-time function

In this section we compare lead-time dependent efficiency and predictability of the different routes R1, R2 and R3. We chose to stick with F5 to model uncertainty conditions.

In Figure 19: Mean delay over lead-time for route R1 (green), R2 (blue), R3 (red) calculated with safety margin 10NM, uncertainty function F5 (AEMET).Figure 19 the influence of the course of the yet to optimize route in the context of the area of convective cells becomes obvious. Route R3 is planned to face the adverse weather through its lateral centre. While the lateral extension of the high-risk area, both in port or starboard direction is big, the deviation will be long and so we will have a poor efficiency right in the beginning. After some forecast steps the deviation is optimized and finally results in a similar magnitude like route R1 and R2 at 131s of delay. That means that the forecasts help to increase efficiency (decreasing mean delay) in this case. For route R2 in blue this is not the case as mean delay fluctuates in a band between 110s and 170s i.e. this route does not benefit from the nowcasts.

Predictability, reflected by the spread of the arrival times, on the other hand shows a different picture. As uncertainty grows with lead-time, spread does as well grow up to finally 589s in case of route R3 (see Figure 20). That means that of all the trajectories that were predicted by DIVMET (M=30 for each lead-time), the minimum one and maximum one differ by almost 10 minutes in arrival time.

It is also noted that while the final mean delays of the predicted trajectories of all routes stay close together around 100s, the spread is very different with values of 102 for R1, 283 for R2 and 589 for R. All graphs of dispersion over lead-time increase but also fluctuate strongly while increasing. This is due to the uncertainty that we put into the DIVMET simulation that causes the convective cells to fluctuate from one forecast lead-time to the next.

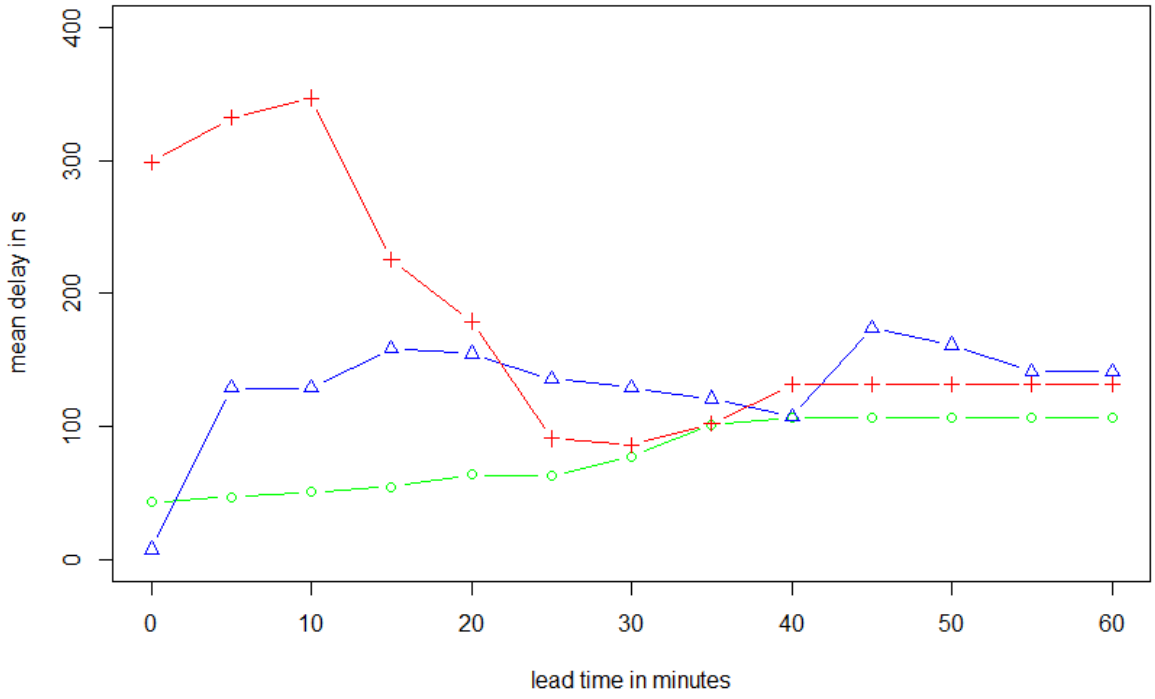

Figure 19: Mean delay over lead-time for route R1 (green), R2 (blue), R3 (red) calculated with safety margin 10NM, uncertainty function F5 (AEMET).

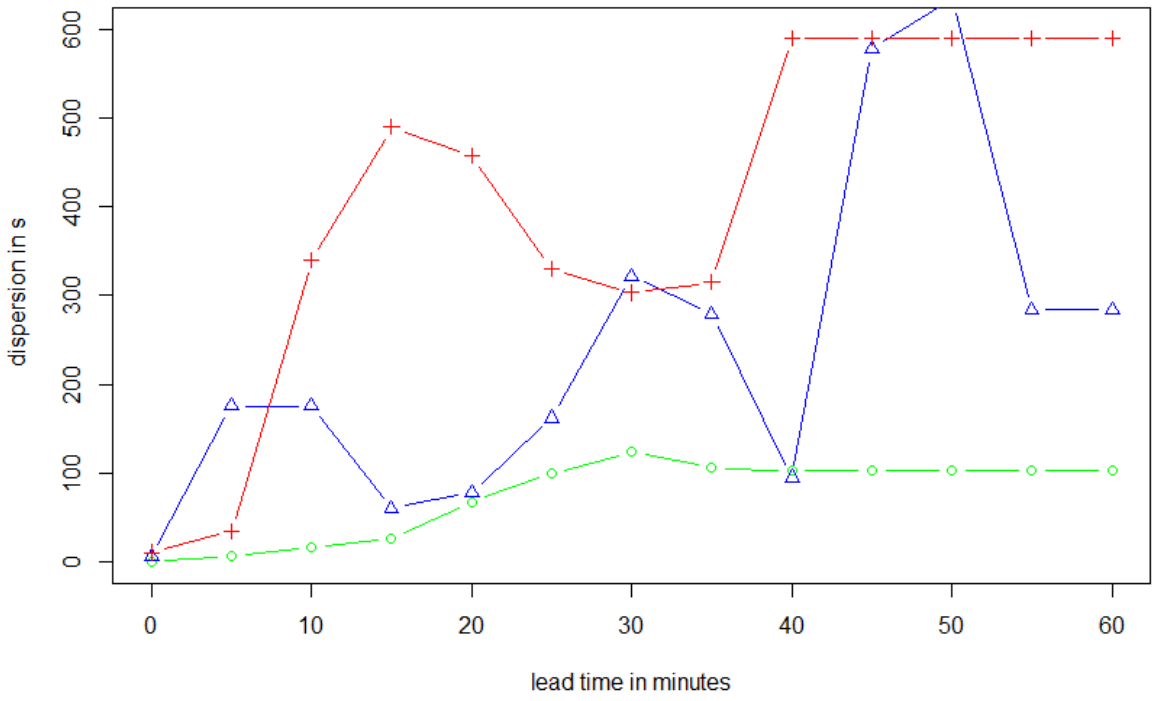

Figure 20: Dispersion (spread) over lead-time for route R1 (green), R2 (blue), R3 (red) calculated with safety margin 10NM, uncertainty function F5 (AEMET).

4 Conclusions

In this deliverable we have presented a first step towards the understanding of the inherent uncertainty of storms, and its consideration for the re-routing of aircraft at the tactical level. The following conclusions can be drawn:

We have introduced a methodology for short-term trajectory prediction that is capable of taking uncertainties of thunderstorm cells into account on the tactical planning level (short term planning and execution). The methodology consists of multiple trajectory predictions under forecast lead-time dependent variation of the field of convective cells. The variation of the convective cells is done by randomly varying the location of the convective cells within a lead-time dependent uncertainty margin. It was found that the methodology is suitable to master the task.

We have derived statistical parameters from the multiple trajectory predictions in order to estimate the effect of uncertainty on predictability and efficiency of the predicted trajectories. This was done in the scope of case studies. The case studies confirmed the working hypothesis that with growing uncertainty the predictability and the efficiency of the predicted trajectories decrease.

The case studies contained the comparison of the results between differently effective uncertainty functions. We found here an apparent dependency of predictability and efficiency under the different uncertainty conditions. A quantification of the uncertainty effects on the results needs a bigger sample size than the three case studies that were analysed in this task.

By the detailed analyses of intermediate results of single trajectory predictions we showed that predictability and efficiency are affected strongly by the course of the DBT in context of the adverse weather zone. Additionally the safety distance that represents the risk awareness of the pilot plays a major role.

Outlook:

Other extensions, which lie out of the scope of TBO-Met and represent some examples of the potential for further development, include:

The modelling of uncertainty of convective cells is aimed to be refined by means of considering the development of the cells in time. To know the potential of build-up and decay of thunderstorm cells within short forecast lead-times may improve trajectory prediction strongly. To do so, available nowcast data has to offer related information.

The results of the DIVMET algorithm may also be improved by using polygons that represent the real shape of thunderstorms instead of using the elliptically shaped approach that we had to use in this study. To do so, available nowcast data has to offer this kind of information.

The number of case studies should be extended in order to increase resilience of the statistics performed here. This may lead to functional relationships between forecast uncertainty and predictability/efficiency of the predicted trajectory.

5 References

[1] T. Hauf, L. Sakiew, M. Sauer, 2013: Adverse weather diversion model DIVMET. Journal of Aerospace Operations 2, pp. 115 - 133. – DOI 10.3233/AOP-130037.

[2] D. Sacher, 2017: Requirements and Concept for Nowcast Processing. TBO-Met D2.3, tech. rep., TBO-Met Consortium.

[3] L. Sakiew, 2016: Flugroutenmodellierung bei Gewitter, PhD-Thesis.

[4] M. Sauer, 2015: On the Impact of Adverse Weather Uncertainty on Aircraft Routing – Identification and Mitigation, PhD-Thesis.

[5] M. Soler, D. González-Arribas, and Manuel Sanjurjo-Rivo, 2017: "Efficiency/Predictability of 4D Trajectories at pre-tactical Level, D4.1, tech rep., TBO-Met Consortium, 2017.

[6] D. Sacher and M. Siegmund, 2017: Software Documentation for Nowcast Processing. TBO-Met D2.3, tech. rep., TBO-Met Consortium, 2017.

[7] "TBO-Met Grant Agreement. Grant number 699294."

[8] D. Rivas, A. Valenzuela, and A. Franco, 2016. "Project Management Plan. TBO-Met's D1.1," D1.1. tech. rep., TBO-Met Consortium, 2016.

6 Appendix - Evaluating convective uncertainty from 2D YRADAR data

6.1 Limitations of the data

The data consists in radar images analysis from the AEMET radar network. The analysis provides areas where it is supposed to be convection, and an estimation of the translation of the convective areas. There is not estimation about:

- change in speed and direction of the displacement of individual cells,
- change in the size of the convective areas,
- new convective cells that can appear in the future,
- the complete track of each convective cell.

Therefore, YRADAR is a useful tool as it helps the forecaster to diagnose the convection and provides an estimation of the movement of the convective cells in the next hour. However, the forecaster uses other sources as: original radar images (PPI, ECHOTOP, MAXREF, VIL), satellite images, SAF products (satellite application facility products), lightning observations, rain gauge data, forecasts from high resolution models in RUC mode (rapid update cycle) and more. Of course, experience provides a knowledge that can add value to the forecasts. As a conclusion, YRADAR analysis is not, by itself, a nowcast. This should be kept in mind, as a limitation of the product being used.

6.2 Data being used

There is an analysis every ten minutes. In each analysis a number of convective cells are detected from the radar images. In turn, for each convective cell, a number of parameters are calculated. Those parameters are written in a text file, such that there is a text file corresponding to each radar image analysis.

The text files are in comma-separated format, so each row corresponds to a convective cell and each column corresponds to a parameter. The first line in each file is a descriptor of the data contained in each column.

We use the following data:

- Latitude and longitude of the center of each convective cell, given in the columns LATCEN and LONCEN of each text file.

- The geographical window where the cell is located, defining a **convective area**, given by LATNOR, LATSUR, LONOES and LONEST.
- The effective radius of each convective cell, RADIOE. The area of the convective cell is the area of a circle with a radius equal to the effective radius. The area of the convective area is greater than the area of the convective cell.
- An estimation of the translation of the convective area: the direction in degrees (departure from North, positive clockwise) and the speed of the translation (in kilometers per hour). These parameters are given by DIRN and VKMH respectively.

Some definitions and remarks:

- A **convective area** is defined as the geographical window where the convective cell is located. It is determined by the values of LATNOR, LATSUR, LONOES and LONEST.
- We do not know the shape of the convective cells, because the application does not save this information. In this work we do not make any assumption about the shape of the convective cells inside each convective area. We could say that the probability of finding convection in a convective area is given by the quotient of the area of the convective cell by the area of the convective area.
- In this work we are interested in the forecast of **convective areas**, not in the convective cells. Moreover, we are interested in providing a **probabilistic forecast** of convective areas. However, the data used is deterministic in nature: a unique estimation of the location and the translation of each convective area.
-

6.3 Problem and possible solution

Therefore, we face the challenge of providing a probabilistic forecast from a deterministic forecast. Trying to stay as simple as possible, we are going to use a training set of forecasts to provide a probabilistic forecast using the following method. Suppose there is a system which, after an experiment, can be in two **states**, $S = \{A, A^*\}$. On the other hand, the experiment can be done in three different conditions or **exclusive categories**, C={α_1, α_2, α_3}. The categories are characterized arbitrarily following a set of rules. As we will see later, thsee categories are supposed to have a predictive value, and therefore are part of a **forecast method**. We repeat the experiment a big number of times N and construct the following **contingency table (Table 4)**:

	C=α_1	**C=α_2**	**C=α_3**
S=A	N(A,α1)	N(A,α2)	N(A,α3)
S=A*	N(A*,α1)	N(A*,α2)	N(A*,α3)

Table 4: Contingency table.

In this table, N(A,α1) is the number of experiments that resulted in the state A and were characterized in the category α1. The other numbers of the table are interpreted similarly.

As mentioned, the characterization rules that permit a classification of the experiments in a set of categories can be used as a prediction method. This is done by introducing the conditional probability: the purpose is to know which is the probability of obtaining a state A, when the experiment was done in a given exclusive category α_k. These probabilities can be estimated as

$$p(S = A|C = \alpha_k) = \frac{N(A, \alpha_k)}{N(A, \alpha_k) + N(A^*, \alpha_k)} \quad (1)$$

Then, the contingency table between states of the experiment and categories with predictive value can provide a **probabilistic forecast**.

The translation of this methodology to our problem, that is, the probabilistic forecast of convection in a given area, can be done in many different ways. We follow the rule of simplicity, leaving open the door for more complicated assumptions.

We use the following definitions:

- The **experiment** consists in evaluating if a given location (defined by the latitude and longitude) is inside a **convective area** at a given moment. The convective area was previously defined by a geographical window, a direct output of the AEMET application that analyzes radar images.
- The **states** of the experiment are, logically, that the location is inside a **convection area** or it is not. As mention before, we do not make any assumption about the shape of the convective cell inside each convective area.
- The **categories** that are supposed to have **predictive value** are defined taking into account two factors: the **forecast range** and the **distance of the location to a convective area** as predicted by the AEMET radar image analysis.
- The **probabilistic forecast** consist in determining the probability that a given location is inside a convective area, provided the forecast range and the distance to a convective area predicted by the AEMET application. That is, we make the assumption that the probability of encountering convection depends on the forecast range and the distance to the predicted convective area.
-

6.4 Data used for finding the contingency tables

	Forecast category
Observed A	a =5.129e+09 km^2
Observed A*	b =7.762e+06 km^2

Table 5: Example of the results for a forecast category. In this table the category corresponds to all the locations at a distance between 1818 and 2020 km from a predicted convective area with a lead-time of 20 minutes. In the table A means *convective area*, and A* means *no convective area*. Within this category there were a = 5.129e+09 km^2 of observed *convective area* and b 7.762e+06 km^2 of observed *no convective area*.

Due to the computational cost, a limited number of days were used for finding the contingency tables. The selected days, with high convective activity, are 2016/12/15, 2016/12/16, 2016/12/17,

2016/12/18, 2016/12/19, 2017/01/20, 2017/01/21, 2017/02/03, 2017/02/04, 2017/03/24, 2017/03/31, 2017/04/25, 2017/05/05, 2017/05/09, 2017/05/10, 2017/05/11, 2017/05/18, 2017/05/25, 2017/05/26 and 2017/05/28.

distance (km)	0 min	10 min	20 min	30 min	40 min	50 min	60 min
0	1.000	0.566	0.403	0.298	0.227	0.177	0.140
2	0.000	0.257	0.218	0.179	0.147	0.122	0.102
4	0.000	0.149	0.160	0.143	0.124	0.107	0.092
6	0.000	0.085	0.114	0.114	0.104	0.094	0.083
8	0.000	0.048	0.081	0.090	0.088	0.081	0.074
10	0.000	0.027	0.056	0.069	0.072	0.070	0.066
12	0.000	0.017	0.039	0.053	0.060	0.059	0.058
14	0.000	0.011	0.027	0.041	0.049	0.051	0.051
16	0.000	0.007	0.019	0.032	0.039	0.044	0.045
18	0.000	0.005	0.014	0.024	0.032	0.037	0.039
20	0.000	0.004	0.010	0.019	0.026	0.031	0.034
22	0.000	0.003	0.008	0.015	0.021	0.026	0.029
24	0.000	0.002	0.006	0.012	0.017	0.021	0.025
26	0.000	0.002	0.005	0.009	0.014	0.018	0.021
28	0.000	0.002	0.004	0.008	0.011	0.015	0.018
30	0.000	0.001	0.003	0.006	0.010	0.013	0.016
32	0.000	0.001	0.003	0.005	0.008	0.011	0.014
34	0.000	0.001	0.002	0.005	0.007	0.009	0.012
36	0.000	0.001	0.002	0.004	0.006	0.008	0.010
38	0.000	0.001	0.002	0.003	0.005	0.007	0.009

Table 6: Table of probabilities for each category. The categories are defined by the distance to a predicted convective area (rows) and the lead-time (columns). The column for 0 minutes correspond to the analysis, therefore the probability is 1 if the distance is 0 and 0 if the distance is greater. Another example: a point that is at a distance of 5 km from a predicted convective area with a lead time of 30 minutes has a probability of 0.083 to be in a convective area.

Then, for each **forecast range** (0 up 60 minutes hours every 10 minutes), and for each **distance to a predicted convective area** (00 to 3838 km every 22 km), we can count how much of this areas where classified as *convective* and *no convective* according to the observations, that is, the analysis of the YRADAR application.

Now, we are interested in the probability that a given point X will be classified as inside a *convective area* given that it is at a certain distance d of a predicted convective area with a lead-time t. These probabilities can be estimated from Equation (1). That is:

$$p(X = A|C = \{d, t_k\}) = \frac{N(A, \{d, t_k\})}{N(A, \{d, t_k\}) + N(A^*, \{d, t_k\})} = \frac{a}{a + b} \quad (2)$$

where $C\{d, t_k\}$ means the category defined by a distance d and a lead time t. The probabilities $p(X = A|C = \{d, t_k\})$ can be computed from the entries a and b in Table 5. In Figure 21 it is shown an example: the observed convective areas (in red), the predicted convective areas (blue) and the areas at different distances from the predicted areas (in gray, darker gray are nearer).

Finally, the probabilities $p(X = A|C = \{d, t_k\})$ for all the categories are listed in Table 6. These probabilities are plotted in Figure 22. From this figure we appreciate some facts:

- The probability of being in a convective area decreases with the distance to the predicted convective areas, which is a good result. This means that if some point is nearer to a predicted convective area, the probability of being in a convective area is greater.
- The probabilities also depend on the leading time of the forecast. For short distances, under 5 km, the probabilities are higher for shorter leading times, which is also an expected result. In between distances from 5 to 10 km the probabilities are similar, near 0.1, for all the leading times. For distances greater that 10 km shorter leading times have lower probabilities.
- These results indicate that forecasts are better for shorter leading-times (as expected), and also permits to quantify the probability of occurrence of convection in a point, as a function of the distance to a predicted convective area with a given leading time.

From the verification exercise we can provide an uncertainty margin for each forecast range. The function F5 presented in Section 3.1 is found from the probabilities given in Table 6 and plotted in Figure 22.

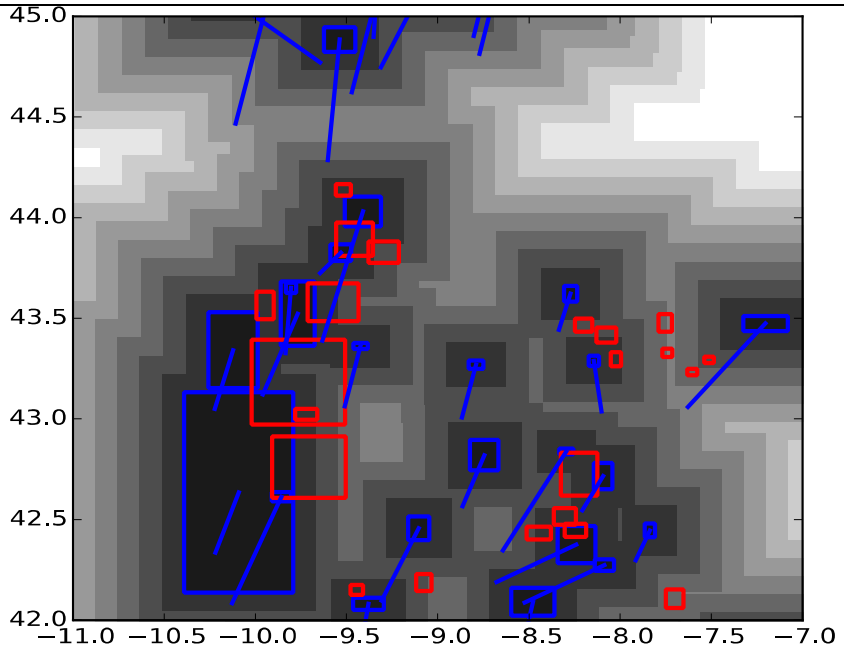

Figure 21: Red boxes: observed convective areas at time t = 1 hour. Blue boxes: predicted convective areas for t = 1 hour, made 1 hour before, that is, at t = 0. Blue lines: movement of the centers of the predicted convective areas, from t = 0 to t = 1 hour. Gray scales: areas which are at different distances from the predicted convective areas (blue boxes). Gray areas are used in the verification process for defining the categories.

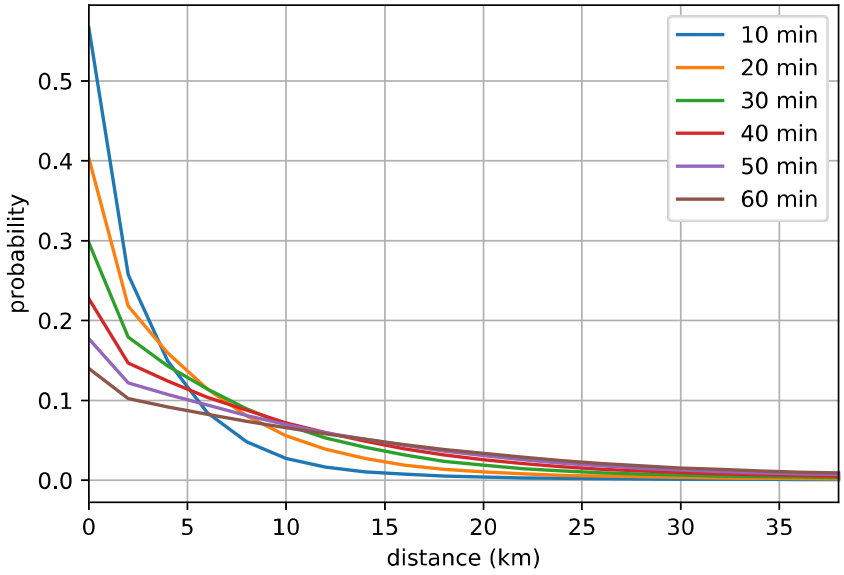

Figure 22: Probabilities from Table 6. Each curve corresponds to a forecast lead time, from 10 minutes up to 60. The probability of being in a convective area decreases with the distance to a predicted convective area. The curves are different for different leading times.